

Journal of Geophysical Research: Oceans

RESEARCH ARTICLE

10.1002/2016JC011977

Key Points:

- Dates of seasonal sea ice retreat and advance in the Chukchi Sea are strongly correlated with variability in the Bering Strait heat inflow
- Ocean heat uptake and albedo feedback provide an additional source of predictability of the date of sea ice advance
- Predictability of the open water period in the Chukchi Sea will be limited by the high variability in summer weather conditions

Correspondence to:M. C. Serreze,
serreze@nsidc.org**Citation:**

Serreze, M. C., A. D. Crawford, J. C. Stroeve, A. P. Barrett, and R. A. Woodgate (2016), Variability, trends, and predictability of seasonal sea ice retreat and advance in the Chukchi Sea, *J. Geophys. Res. Oceans*, 121, 7308–7325, doi:10.1002/2016JC011977.

Received 18 MAY 2016

Accepted 15 SEP 2016

Accepted article online 19 SEP 2016

Published online 4 OCT 2016

Variability, trends, and predictability of seasonal sea ice retreat and advance in the Chukchi Sea

Mark C. Serreze¹, Alex D. Crawford¹, Julienne C. Stroeve¹, Andrew P. Barrett¹, and Rebecca A. Woodgate²

¹National Snow and Ice Data Center, Cooperative Institute for Research in Environmental Sciences, University of Colorado Boulder, Boulder, Colorado, USA, ²Applied Physics Laboratory, University of Washington, Seattle, Washington, USA

Abstract As assessed over the period 1979–2014, the date that sea ice retreats to the shelf break (150 m contour) of the Chukchi Sea has a linear trend of -0.7 days per year. The date of seasonal ice advance back to the shelf break has a steeper trend of about $+1.5$ days per year, together yielding an increase in the open water period of 80 days. Based on detrended time series, we ask how interannual variability in advance and retreat dates relate to various forcing parameters including radiation fluxes, temperature and wind (from numerical reanalyses), and the oceanic heat inflow through the Bering Strait (from in situ moorings). Of all variables considered, the retreat date is most strongly correlated ($r \sim 0.8$) with the April through June Bering Strait heat inflow. After testing a suite of statistical linear models using several potential predictors, the best model for predicting the date of retreat includes only the April through June Bering Strait heat inflow, which explains 68% of retreat date variance. The best model predicting the ice advance date includes the July through September inflow and the date of retreat, explaining 67% of advance date variance. We address these relationships by discussing heat balances within the Chukchi Sea, and the hypothesis of oceanic heat transport triggering ocean heat uptake and ice-albedo feedback. Developing an operational prediction scheme for seasonal retreat and advance would require timely acquisition of Bering Strait heat inflow data. Predictability will likely always be limited by the chaotic nature of atmospheric circulation patterns.

1. Introduction

The sharp decline in end-of-summer Arctic sea ice extent over the period of satellite observations (1979–present) is one of the most visible indicators of our planet's changing climate. This ice loss is already having ecological impacts [Post *et al.*, 2013]. Loss of the ice cover has promoted stronger solar heating of the ocean mixed layer during spring and summer, acting to delay autumn ice growth [e.g., Perovich *et al.*, 2007; Steele *et al.*, 2008; Stammerjohn *et al.*, 2012; Stroeve *et al.*, 2014]. Enhanced heat fluxes from the ocean back to the atmosphere in autumn and winter is a major driver of Arctic amplification—the outsized rise in Arctic surface air temperatures relative to the rest of the globe [Serreze *et al.*, 2009; Screen and Simmonds, 2010]. Whether the effect of ice loss on Arctic amplification extends through a deep enough layer of the troposphere to alter jet stream patterns with impacts on middle-latitude weather is a vibrant area of debate [e.g., Francis and Vavrus, 2012; Tang *et al.*, 2013; Perlitz et al., 2015].

What is not in doubt is that continued sea ice loss will make the Arctic Ocean increasingly accessible for oil and natural gas exploration and development, marine transport, tourism, and other activities [United States Navy, 2014]. There is hence a need for a better understanding not only of the evolution of the sea ice cover on decadal and longer scales, but also on seasonal time scales that bear directly on economic activities. Predicting the seasonal onset and duration of open water on a regional basis is of particular importance, and the Chukchi Sea stands out in this regard (Figure 1). This shallow sea, which has seen some of the sharpest downward trends in September ice extent over the satellite record [e.g., Comiso, 2012], is a focus of resource exploration, and vessels transiting the Arctic Ocean must invariably pass through it. The Chukchi Sea is also part of the seasonal migration route for bowhead whales that supports subsistence hunting [Moore and Laidre, 2016].

Developing a predictive capability for the Chukchi Sea requires understanding the factors that control both the date of summer ice retreat and the date of autumn ice advance. These issues are addressed from an observational perspective through first examining observed trends, and then using detrended time series to document

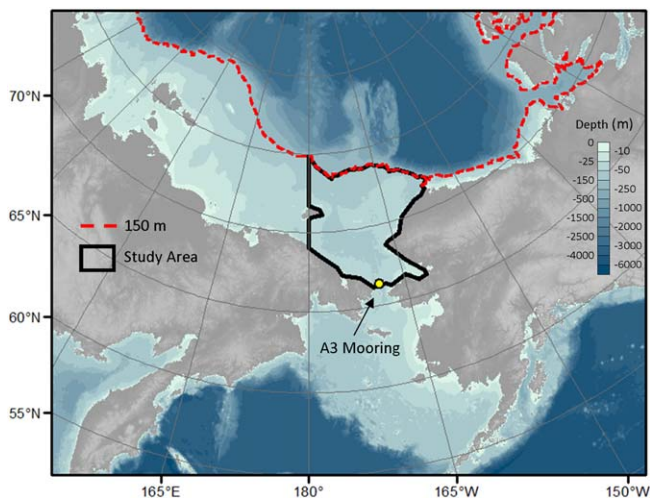


Figure 1. Location map showing the Chukchi Sea as defined in this study and bathymetry. The dotted red line shows the 150 m isobath. The region has an area of 511,250 km². The location of the A3 mooring is also shown.

tion and extent from 1979 through the present at 25 km resolution on a polar stereographic grid by combining data from the Nimbus-7 Scanning Multichannel Microwave Radiometer (SMMR, 1979–1987), the Defense Meteorological Satellite Program (DMSP) Special Sensor Microwave/Imager (SSM/I, 1987–2007), and the Special Sensor Microwave Imager/Sounder (SSMIS, 2007–onward). The present study utilizes daily time series for the period 1979–2014 available from the National Snow and Ice Data Center, based on the National Aeronautics and Space Administration team algorithm [Fetterer *et al.*, 2002].

Before calculating the open water period, the daily sea ice concentration was averaged for the entire Chukchi Sea shelf sector, as defined in Figure 1. The adopted southern, eastern, and western geographic boundaries of the Chukchi Sea shown in Figure 1 are the same as used in the National Snow and Ice Data Center Multisensor Analyzed Sea Ice Extent product (<https://nsidc.org/data/masie/>). However, the northern boundary is taken as the 150 m isobath, which restricts analysis to the continental shelf sector where resource exploration is focused. Each grid cell is weighted by area when taking the average. The beginning of the open water period, termed the retreat date, is defined as the first day of the year when the average sea ice concentration within this sector is less than 30%. The end of the open water period, termed the advance date, is the first day after the seasonal ice extent minimum when the average sea ice concentration in this sector exceeds 30%. The open water period is simply the difference between the two dates. The 30% threshold was chosen because it allows ice retreat and advance dates to be calculated for every year. A 15% concentration threshold, commonly adopted in the research community in studies of ice extent, was found to be undesirable as there were some years, early in the record, where the average concentration in the Chukchi Sea never fell below 15% (or even 25%). Using a 15% threshold would mean throwing out data for some of the earlier years when sea ice was more extensive, leading to a bias in our statistical analyses.

2.2. Sea Ice Motion and Age

Arctic-wide estimates of sea ice motion and age are available for the period 1982–2014, derived from an algorithm applied to a combination of satellite passive microwave data, visible and thermal imagery, and drifting buoys [Fowler *et al.*, 2004]. Ice motion is calculated from a cross-correlation technique applied to sequential daily satellite images. These motion fields are then blended with buoy drift vectors via optimal interpolation to create the final motion product. Ice age is estimated by treating each grid cell that contains ice as an independent Lagrangian particle and advecting the particles at weekly time steps and using an ice concentration threshold of 15%. At the end of each melt season, remaining ice is aged 1 year. A grid cell is assigned the age of the oldest “particle” that lies in the domain of that grid cell. Fowler *et al.* [2004] and Maslanik *et al.* [2007, 2011] provide further details. The value of ice age is that from a thermodynamic point of view, older ice classes tend to be the thicker ice classes, and therefore are more resistant to melting out during summer. The ice age data set hence provides at least a sense of variability and change in thickness

(a) an important relationship between both sea ice retreat and advance and variability in the Bering Strait heat inflow as estimated from in situ mooring data; (b) the influence of both long-wave and shortwave radiation on the retreat and advance dates; (c) the role of local seasonal ocean heat uptake and albedo feedback in providing an additional source of predictability of the advance date; and (d) the role of variable summer atmospheric patterns in limiting potential predictability.

2. Data and Methods

2.1. Sea Ice Retreat, Advance, and Open Water Period

The satellite passive microwave record provides estimates of ice concentration

extending over a longer time period than possible from satellite altimeter or aircraft altimeter retrievals (or other sources). All ice that has survived at least one melt season (second year and older) is defined as multi-year ice. The obvious limitation in linking ice age and thickness is that thick ice can also result from ridging.

2.3. Ocean Heat Transport

We use estimates of monthly averaged ocean heat transport (cited in TW) through the Bering Strait from the A3 mooring for the periods September 1990 through September 1992 and August 1997 through December 2013 (minus June 1999). The A3 mooring, located at approximately 66.33°N, 168.96°W, ~35 km north of the Bering Strait proper (see Figure 1), is part of a larger mooring project to assess water properties and fluxes of heat, salt, and total water volume through the strait [Woodgate *et al.*, 2015], currently supported by the NSF-Arctic Observing Network program. Maintaining the mooring array is logistically challenging and the gap in A3 coverage between October 1992 and July 1997 reflects these challenges and prior modifications of the array. The heat fluxes used here are calculated from lower layer (~45 m depth) measurements of temperature and velocity at mooring site A3 [Woodgate *et al.*, 2010]. Fluxes are calculated relative to -1.9°C , the freezing point of Bering Strait waters, because Bering Strait waters leaving the Arctic are typically around freezing [Steele *et al.*, 2004], and thus the calculation yields the total heat lost from these waters between entering and the leaving the Arctic, either to melting ice or to warming the atmosphere or other waters. Although we cannot be certain of the fate of this heat, a large fraction (order 3/4) of this heat is lost by the time the waters reach the offshelf Chukchi Sea (e.g., compare offshelf data (yellow curve) with Bering Strait data in Woodgate *et al.* [2012, Figure 3] or Timmermans *et al.* [2014, Figure 16]).

The calculated heat flux from A3 data underestimates the total Bering Strait heat flux, but because of its location, the values should be well correlated with the total flux and provide a good sense of its interannual variability. The reason that the A3 calculation above underestimates the total heat flux is because it does not capture the contribution from the seasonal (warm) Alaskan Coastal Current (ACC, see later discussion) and the effects of vertical stratification of the water column [Woodgate *et al.*, 2015]. Stratification refers to the observed summer to late autumn, approximately two-layer structure of the water column, with a seasonal upper warmer (and typically) fresher layer 10–20 m thick that is found throughout the strait, and a lower layer that tends to be cooler and saltier [Woodgate *et al.*, 2012, 2015]. Below, where we require total heat fluxes, we add a standard correction for these terms (see Woodgate *et al.* [2010] for discussion).

2.4. Atmospheric Conditions

For analysis of atmospheric conditions, 1979–2014, reliance is placed on data from two reanalysis products (a) MERRA (the Modern Era Retrospective-analysis for Research and Applications) [Rienecker *et al.*, 2011] and (b) ERA-Interim (European Reanalysis Agency) [Dee *et al.*, 2011]. Atmospheric reanalyses like MERRA and ERA-Interim represent retrospective forms of numerical weather prediction, using a fixed model and data assimilation system. Analyzed fields (analyses) such as pressure heights, winds, temperature, and specific humidity at standard atmospheric levels represent the blending of a short-term atmospheric forecast with observations from radiosondes, satellite sounders, aircraft reports, and other sources. Each analysis cycle consists of collection, selection, and quality control of observations available within the analysis window; assimilating the observations into a first guess of the state of the atmosphere (the short-term forecast) using a statistical interpolation scheme; dynamically balancing the analysis; and integrating the forecast model forward in time to the beginning of the next analysis cycle. The new forecast is used as the first guess for the next analysis cycle. Surface fields, such as 2 m air temperature, precipitation, and surface radiation fluxes, are generated as part of the forecast step. The MERRA analysis is performed at a horizontal resolution of $2/3^{\circ}$ longitude by $1/2^{\circ}$ latitude at 72 levels. ERA-Interim has 60 vertical levels with a spatial resolution of approximately 80 km.

Analyzed fields from different reanalyses tend to be in good agreement with each other. As such, we make use of analyzed fields of sea level pressure (SLP) and temperature at the 925 hPa only from MERRA. During summer, the 925 hPa temperature is preferred over the 2 m temperature because over a melting ice surface, the skin temperature is constant (and at freezing) regardless of energy inputs and there is hence little variability at the 2 m level. The analyzed 925 hPa temperature by contrast provides an indication of the thermal state of the lower troposphere. Note that in MERRA, grid cells with land surface elevations that intersect the 925 hPa level are masked. For examination of links between sea ice advance, retreat and variations in surface fields (radiation fluxes, 10 m winds, 2 m air temperature) comparisons are made between results from MERRA and ERA-Interim. Lindsay *et al.* [2014] evaluated seven different reanalyses in the Arctic

and found that for surface fluxes, MERRA, ERA-Interim, and the NOAA Climate Forecast System Reanalysis tended to perform the best compared to available observations.

2.5. Correlation Analysis and Linear Models

To work toward a predictive capability for sea ice retreat and advance, an analysis of trends and Pearson correlations between sea ice, atmospheric, and oceanic variables in section 4 sets the stage in section 5 for the construction of separate statistical linear models for predicting retreat and advance. Retreat models are constructed using the detrended time series of sea ice retreat day as the predicted variable and all possible seasonal combinations of detrended potential predictors. Potential predictors, taken as April through June averages, include radiation fluxes, air temperature, 10 m meridional (northward) wind velocity, and the Bering Strait heat inflow. The models are based on the 17 years for which all variables are available. In turn, the advance date models use as potential predictors atmospheric variables and the Bering Strait heat inflow for the 17 years averaged from July through September, as well as the date of ice retreat (see later discussion). None of the potential predictors exhibit significant serial autocorrelation from year to year. The Bayesian Information Criterion (BIC), which combines a likelihood function and a penalty for adding parameters that helps prevent overfitting, was used as a measure of model fit [Schwarz, 1978]. The best models were determined as having the lowest average BIC between the two atmospheric reanalyses that also met the following criteria.

1. Predictors are independent, meaning they do not have excessive multicollinearity. (Variance inflation factors were consistently less than 3 in all models examined.)
2. The models explain significantly greater variance in the retreat (and advance) day than all nested models. (The predictors in a nested model are a sub-set of the predictors in the larger model being compared to.)
3. No single observation imposes excessive leverage (based on Cook's distance of 0.5 and leave-one-out experiments).
4. Residuals are normally distributed (based on Q-Q plots) and homoskedastic (based on the Breusch-Pagan test and visual inspection). (If residuals are heteroskedastic, their variance depends on the values of the predictors, which indicates bias in the model.)

Using these criteria ensures that the final models for retreat and advance are not only physically defensible, but also statistically robust. One problem is that the Bering Strait heat inflow exhibits substantial seasonal (but not interannual) autocorrelation which needs to be removed (see section 4.3).

3. Climatological Framework

3.1. Sea Ice Concentration

Even in today's warming climate, the Chukchi Sea is essentially fully ice covered from December through April. At peak coverage, typically mid-March, ice also extends south to cover the Bering Strait and the northern part of the Bering Sea. Surface melt and ice retreat typically start in May, although the continuous melt season generally does not begin until June [Stroeve *et al.*, 2014]. Assessed as median extent for the first day of the months June through November over the period 1979–2014, the satellite passive microwave data (Figure 2) show that at the beginning of June, open water is typically present only in the extreme southern reaches of the shelf region. Seasonal sea ice retreat is largest during July, the warmest month in the Arctic. By the first of July, the ice edge has typically retreated to about 70°N, roughly half way up the Chukchi Sea. As noted by Woodgate *et al.* [2010], the ice edge mimics the northward flow pathways of water through the Chukchi (Figure 2), with preferential retreat along the Alaskan Coast (where the Alaskan Coastal Current is present) and on tongues either side of Herald Shoal (~71°N, 170°W) marking the flow through Herald Canyon and the Central Gap (see Weingartner *et al.* [2005] and Woodgate *et al.* [2005a] for discussion).

Ice coverage is at a minimum in September and almost all the shelf region is open water. However, over the past decade, the September ice edge has been located far north of the continental shelf break. Nearly ice free conditions usually persist into October. Ice growth tends to start by October, progressing generally from north to south. In extreme years, open water may persist into the middle of December. Figure 3 shows the mean seasonal cycle of sea ice concentration in the Chukchi shelf region along with the mean retreat and advance dates based on the 30% concentration threshold. The average open water period is 103 days, and the average retreat and advance dates are July 17 and October 28, respectively, but there is a large range in all three variables, and as already introduced, pronounced trends.

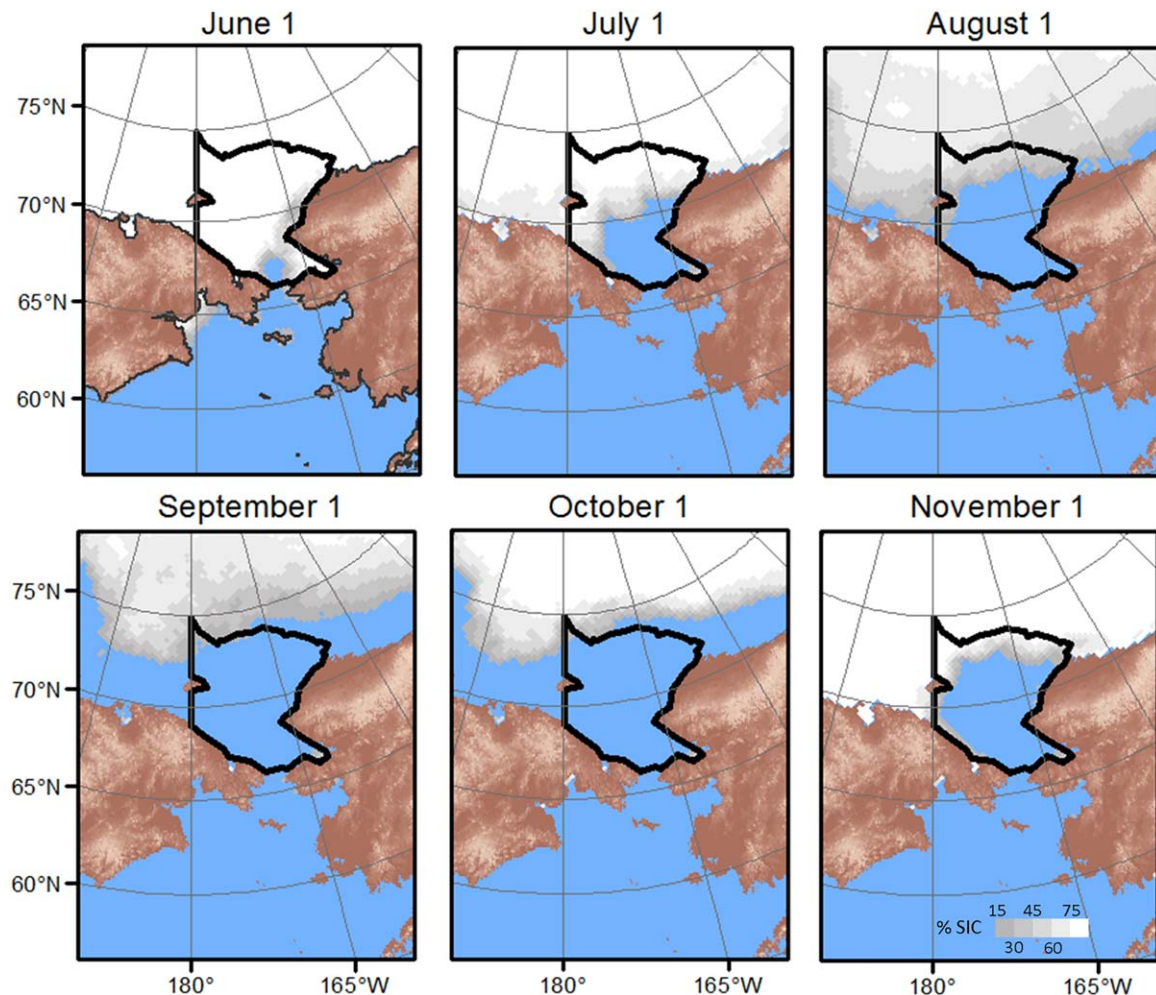


Figure 2. Median ice conditions in the Chukchi Sea shelf region based on the period 1979–2014.

3.2. Atmospheric Circulation, Ice Circulation, and Ice Age

In the annual mean, the Chukchi Sea and the adjacent Beaufort Sea are primarily under the influence of the atmospheric Beaufort Sea High, a mean surface anticyclone centered over the northern Beaufort Sea. The Beaufort Sea High leads to a clockwise pattern of surface winds and hence the ice (and water) motion known as the Beaufort Gyre (Figure 4). Mean annual surface winds and ice drift in the northern parts of the Chukchi Sea are hence westward (from east to west), reflecting the region's location on the southern side of the anticyclone. Generally, thick multiyear ice, generated north of the Canadian Arctic Archipelago through convergence and shear, is transported via the Beaufort Gyre westward across the Beaufort Sea. However, generally little of this multiyear ice finds its way into the Chukchi Sea and what does is mostly found in the northern part of the domain; this was true even during the cooler Arctic climate of 30 years ago (Figure 5). In other words, throughout the period of satellite coverage, typically most ice in the Chukchi Sea is first-year ice, representing a single year's growth. Multiyear ice extent nevertheless varies from year to year; in 1984 and 1995, multiyear ice covered more than 50% of the Chukchi Sea as we have defined it compared to 10% or less in some recent years. Interestingly, occasional excursions of multiyear ice through Bering Strait are documented in satellite tracking [Babb *et al.*, 2013], and from indigenous observations [Oceana and Kauerak, 2014; Raymond-Yakoubian *et al.*, 2014].

The annual mean pattern (averaged from 1979 to 2014) depicted in Figure 4 masks strong seasonal variations in wind patterns and ice drift. This is illustrated in mean SLP and ice motion fields for the months June through November (Figure 6). During May (not shown), the climatological monthly averaged Beaufort Sea High, with a peak pressure of about 1020 hPa, is centered over the eastern Beaufort Sea. The Chukchi Sea is

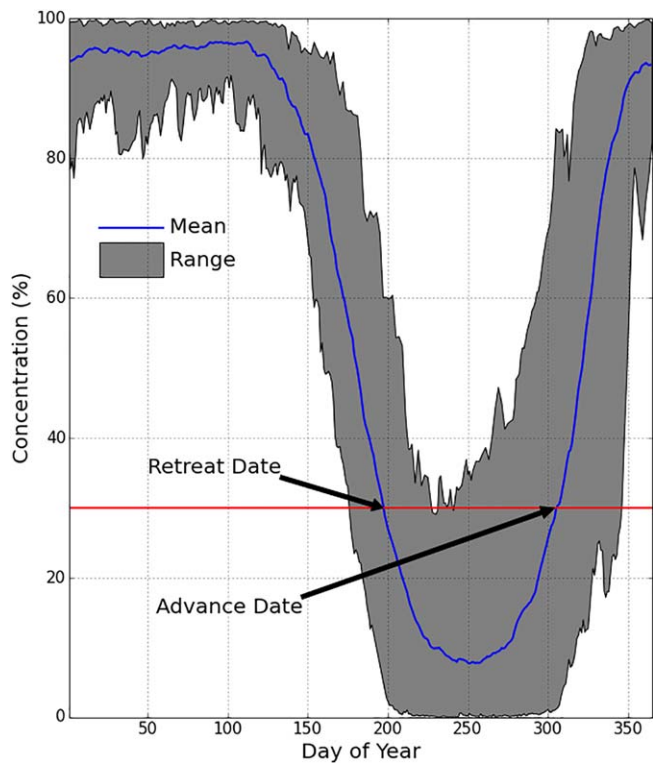


Figure 3. Mean seasonal cycle and range in sea ice concentration in the Chukchi Sea shelf region, and the mean retreat and advance dates based on the 30% sea ice concentration threshold (based on the period 1979–2014).

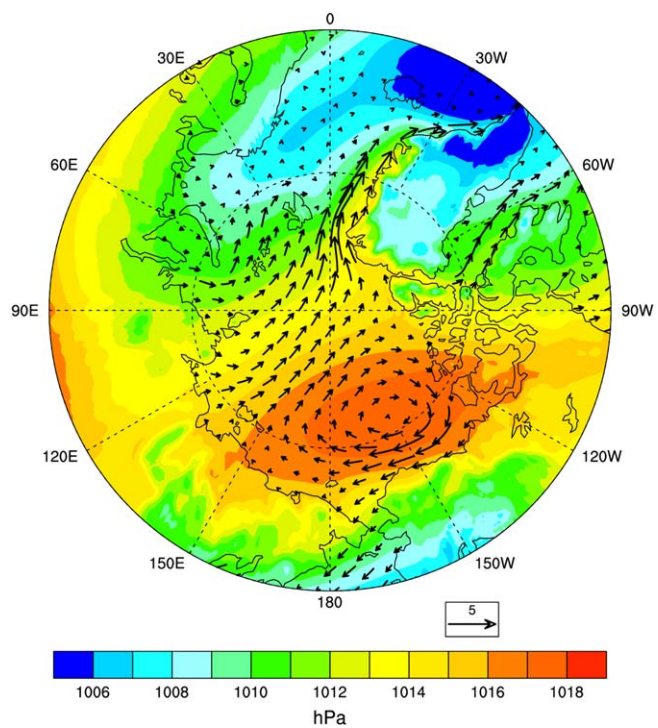


Figure 4. Mean annual sea level pressure (1979–2014) with overlay of sea ice velocity (1982–2014), in cm s^{-1} .

on average an area of weak winds at this time (and hence weak ice drift) with a northward component. The Beaufort Sea High is even weaker in June, and monthly average ice velocities in the Chukchi Sea are mostly less than 2 cm s^{-1} . In August, the pressure field is quite flat, with a weak mean low centered near the pole, promoting a small eastward drift of ice in the Chukchi Sea. Pressures over the Beaufort and Chukchi seas rise from September through October and November, and the counterclockwise Aleutian Low to the south also deepens. Together, this results in increasingly strong pressure gradients and westward (east to west) winds and ice drift in the Chukchi Sea. Of course, for any given year, patterns may depart strongly from those shown in Figure 6. Overland [2009] and Serreze and Barrett [2011] provide an in-depth analysis of the characteristics and variability of the Beaufort Sea High. The summertime Beaufort Sea High exhibits considerable decadal variability. As shown in several recent studies [Moore, 2012; Overland *et al.* 2012; Wu *et al.*, 2014; Serreze *et al.*, 2016], the summer anticyclone has also strengthened since the late 1990s.

3.3. Bering Strait Heat Inflow

Woodgate *et al.* [2015] provide a review of the Bering Strait volume, salinity, and heat inflow based on mooring measurements. The volume transport through this shallow (50 m) and narrow (85 km) strait, split roughly in the middle by Big and Little Diomede islands, is believed to be driven by a difference in oceanic pressure (often called the “pressure head”) between the Pacific and the Atlantic Ocean, the flow being strongly modulated by local wind patterns [Woodgate *et al.*, 2005a]. Dominant features of the inflow are warm and fresh waters along the Alaska side of the strait (east of the Diomede islands) that originate from the ACC, with generally colder waters to the west (the Russian channel). There is a strong

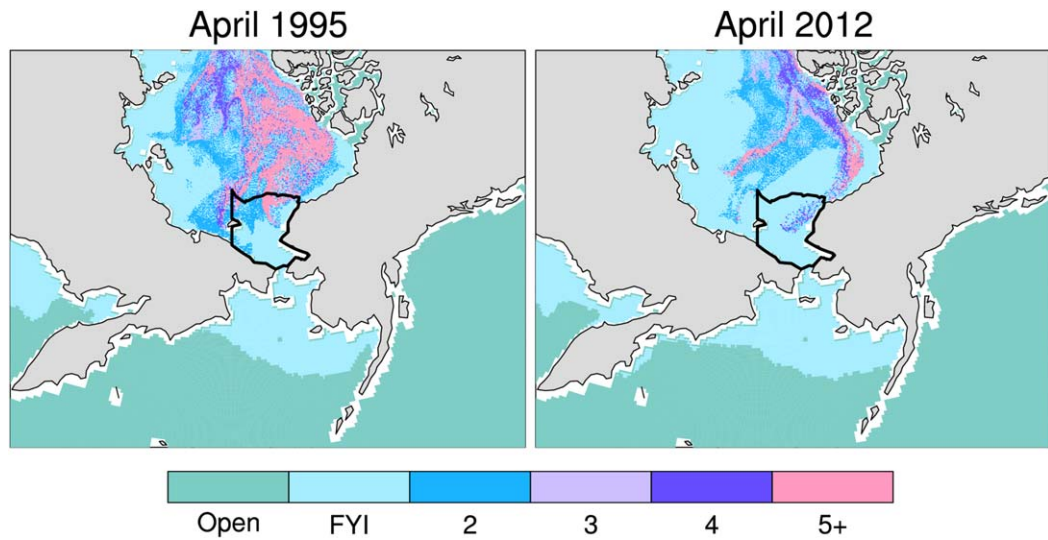


Figure 5. Ice age (in years) for April 1995 and April 2012.

east to west salinity gradient, with the saltier waters on the Russian side of the strait. As discussed earlier, throughout the strait, the water column has a seasonally two-layer structure, with an upper warmer (and typically) fresher layer 10–20 m thick. Likely related, the ACC is also a seasonal feature, present from late April through December. Its freshness and warmth point to a strong influence of river input, especially from the Yukon and the Gulf of Alaska [Aagaard *et al.*, 2006]. The ACC is a narrow (10–20 km wide) feature.

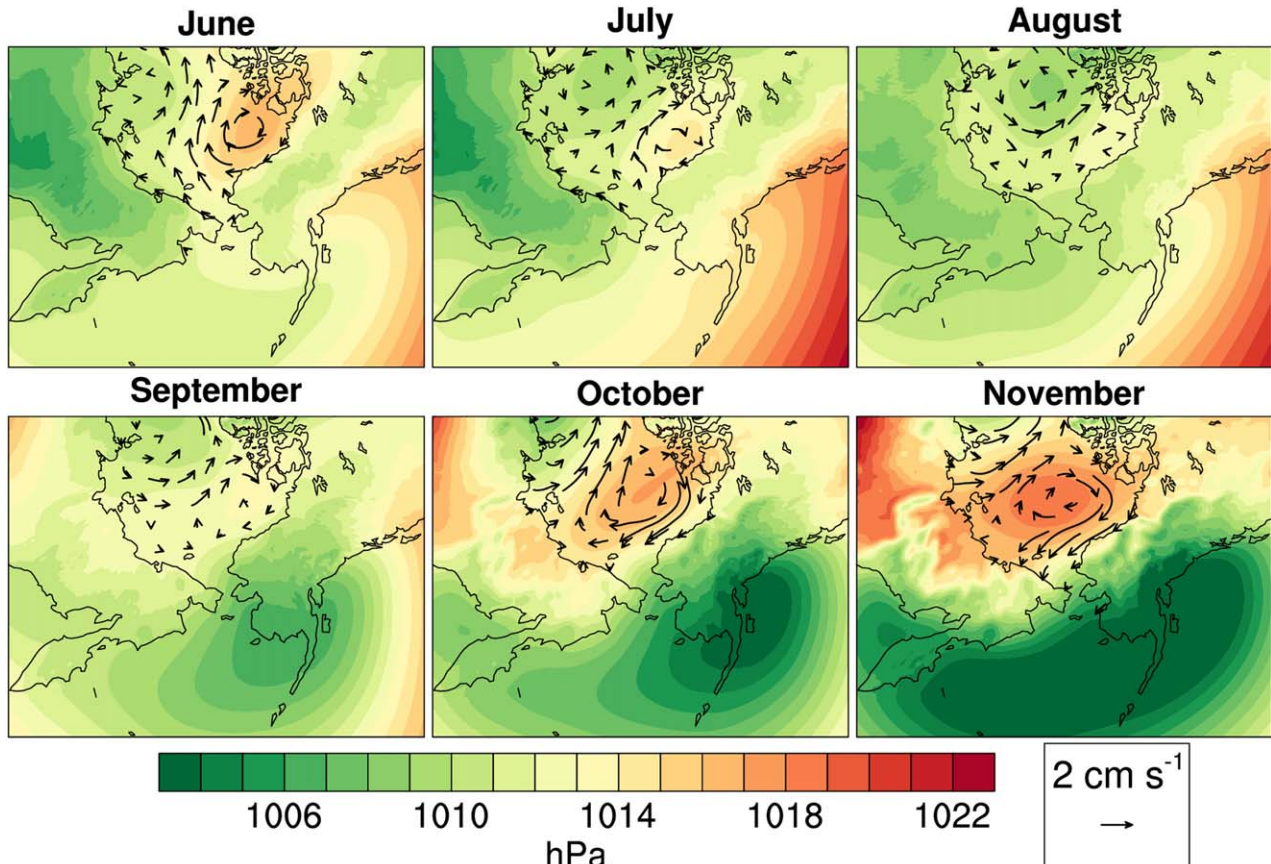


Figure 6. Mean sea level pressure fields and ice velocity vectors, based on the period 1979–2014.

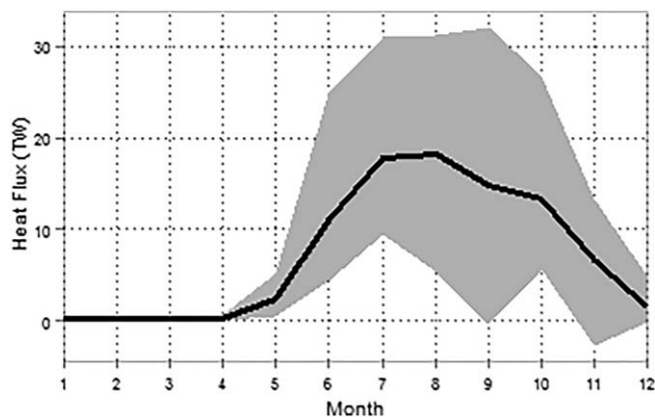


Figure 7. Mean seasonal cycle (solid line) and range in monthly values (shading) of the Bering Strait heat inflow (TW) from the A3 mooring (excluding adjustments for the ACC and stratification) averaged for the 17 years of available data.

in winter and maxima typically in August or September, but as early as June and as late as October (Figure 7). The maximum is driven by both the higher water temperatures in summer as well as a general summer maximum in water volume transport [Woodgate *et al.*, 2005b]. In providing a near-surface heat source, the Bering Strait inflow has long been implicated in the seasonal melt back of ice in the Chukchi Sea region [Fedorova and Yankina, 1963; Paquette and Bourke, 1974; Ahlnas and Garrison, 1985; Spall, 2007; Woodgate *et al.*, 2010, 2015].

4. Retreat, Advance, and Open Water Period

4.1. Trends

Figure 8 shows the time series of sea ice retreat, advance, and the open water period, along with linear trend lines. Also displayed is the time series (including the standard correction for stratification and the ACC) and trend line for the annual Bering Strait heat inflow. The date of Chukchi ice retreat has a linear trend of -0.70 days per year. From the regression line, this equates to about 25 days over the satellite sea ice record (1979–2014). By comparison, the date of ice advance has a steeper linear trend of 1.52 days per year (more than twice as large). This equates to a total change of 55 days. These changes yield a linear trend in the open water period of 2.22 days per year, equating to a total change of 80 days since 1979. The obvious conclusion is that the increasing open water period results more from the trend toward a later advance day than from the earlier retreat day. Woodgate *et al.* [2012] show that between 2001 and 2011, the Bering Strait inflow has increased (both the volume and heat flux), with about one third of the volume flux increase likely explained by weaker local winds, with the remaining two thirds attributed to an increase in the pressure head difference between the Pacific and Atlantic. As assessed over the period 1998–2013 of Figure 8, there is a positive trend in the annual Bering Strait heat inflow from the A3 data of 5.5×10^{18} J/yr.

4.2. Correlations With Retreat Day

Table 1 shows linear correlations between the detrended time series of retreat, and detrended April through June time series of variables that have plausible physical links with retreat and advance (and hence the open water period). Radiation fluxes are defined as positive downward and negative upward. While an alternative is to choose time windows for each variable yielding the highest correlations with retreat and advance, a fixed time window for all variables has the advantage of simplicity and consistency. Results are provided for both the period of coverage from the two reanalyses (1979–2014) and for the 17 year period when Bering Strait heat inflow data are available for all months. We focus first on the period 1979–2014.

Not surprisingly, Table 1 shows statistically significant negative correlations between the retreat day and 2 m temperature based on data from both reanalyses (-0.43 with MERRA, -0.42 with ERA-Interim). The downwelling longwave radiation flux has a significant negative correlation with retreat, whereas the downwelling shortwave flux has a positive correlation (but only significant using the MERRA record), meaning that earlier retreat is associated with more downwelling longwave but less downwelling shortwave. In

Although the volume transport from the ACC is small (~ 0.1 Sv) compared to the total volume transport through the Bering Strait (climatologically ~ 0.8 Sv, more recently ~ 1 Sv [Woodgate *et al.*, 2015]), it is estimated to carry about a third of the heat and about a quarter of the total freshwater flux of the strait [Woodgate *et al.*, 2005b].

The Bering Strait heat inflow as estimated (see section 2.3) from the mid-channel A3 mooring (termed by Woodgate as the “climate site” as it provides a useful average of water properties in the two channels of the strait), displays a very pronounced seasonal cycle, with minimum values

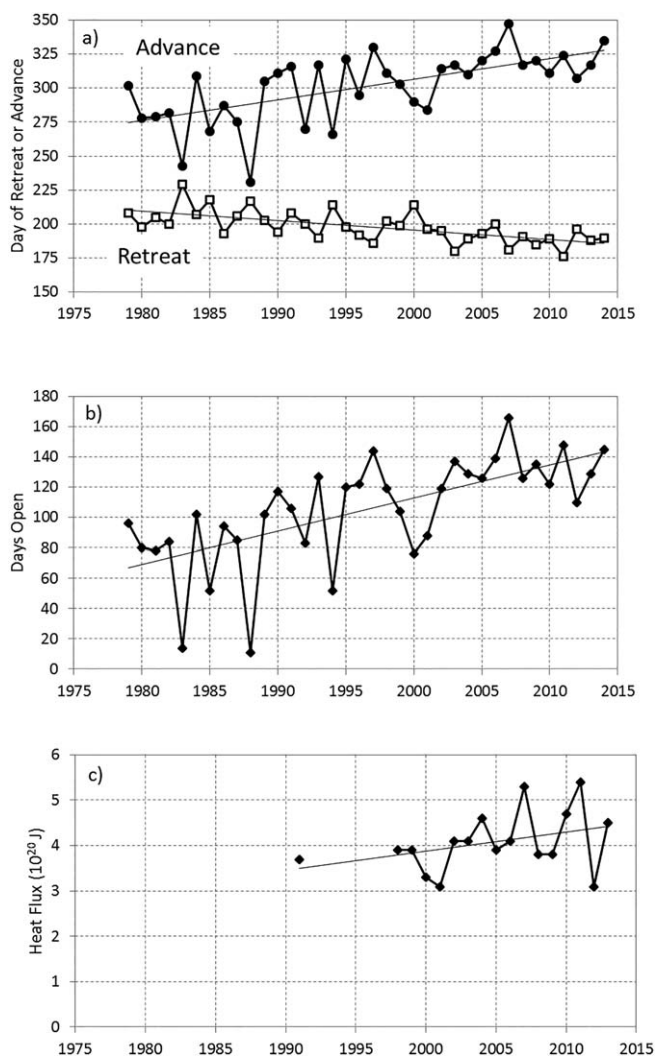


Figure 8. Time series and linear trends for the Julian Day of sea ice retreat and advance, the open water period in days and the Bering Strait heat inflow (including standard corrections for a 20 m surface layer and the ACC as per Woodgate *et al.* [2010]), in 10^{20} J.

to favor an earlier retreat because (a) such winds tend to be warm and to be pushed northward off of the Chukchi shelf. A northward wind also typically increases the northward flow in the Bering Strait [Woodgate *et al.*, 2005a, and references therein], increasing the volume flux and, when water temperatures are above freezing, the heat flux as well. However, Table 1 shows no significant correlation between spring meridional wind and retreat based on both the MERRA and ERA-Interim records. This is perhaps because Table 1 averages the wind over the entire Chukchi Sea. Prior work [Woodgate *et al.*, 2005a] shows that away from the Bering Strait itself, the relationship between local wind and water flow is much weaker.

As part of our analyses, we also examined correlations between the retreat day and the detrended time series for the Chukchi Sea multiyear ice fraction at the end of March, April, and May (months preceding the melt season). In all cases, correlations were found to be quite low and not statistically significant. Given that it takes less energy to melt out thin ice than thick ice, this is perhaps surprising, if one assumes that multiyear ice is typically thicker than seasonal ice. However, ridging of sea ice complicates that assumption. The low correlations between retreat date and multiyear fraction may also reflect that most of the multiyear ice tends to be located in the northern part of the domain (Figure 5), and therefore will play little role in the seasonal pattern of ice retreat, which begins in the southern part of the region covered mostly by first year ice.

Correlations shown in Table 1 between retreat and atmospheric variables for the 17 years with Bering Strait heat inflow data are generally similar to those for the longer (1979–2014) period. However, correlations

explanation, in spring, the cloud radiative effect over the Arctic Ocean is positive, meaning that the increase in the downwelling longwave flux under cloudy skies (which also tends to be associated with more water vapor) more than compensates for the decrease in the downwelling shortwave flux [Curry and Ebert, 1992]. It hence follows that under cloudy skies and high humidity, sea ice will tend to retreat earlier [Kapsch *et al.*, 2016; Mörn *et al.*, 2016].

The strong negative correlations with upwelling shortwave reflect variations in surface albedo—later retreat means more ice and a higher albedo. In turn, more upwelling longwave (more negative values) means a warmer surface, implying less ice. The upwelling fluxes are hence largely responses to variability in sea ice retreat rather than drivers of it. The correlations with the net radiation terms therefore represent a mixture of forcing and response; as seen in Table 1, there are negative correlations between sea ice retreat and all three net radiation variables (net shortwave, net longwave, and net allwave, which is net shortwave plus net longwave). As they represent a mixture of forcing and response, the upwelling and net radiation terms are inappropriate for use in statistical models predicting the timing of ice retreat.

One might hypothesize that winds with a strong northward component ought

Table 1. Pearson Correlations Between Detrended Time Series of Retreat Day and Seasonal Oceanic, Surface Radiation, and Atmospheric Variables Averaged for April Through June^a

Variable	Full Record (1979–2014)		1991–1992, 1998, 2000–2013	
Bering Strait heat inflow		N/A		−0.81 (0.000)
10 m meridional wind	MERRA	ERA-Interim	MERRA	ERA-Interim
2 m temperature	−0.29 (0.08)	−0.29 (0.09)	−0.11 (0.66)	−0.12 (0.64)
Net allwave radiation	−0.43 (0.01)	−0.42 (0.01)	−0.60 (0.01)	−0.59 (0.01)
Net shortwave radiation	−0.66 (0.00)	−0.74 (0.00)	−0.59 (0.01)	−0.66 (0.00)
Downwelling shortwave radiation	−0.39 (0.02)	−0.56 (0.00)	−0.47 (0.06)	−0.52 (0.03)
Upwelling shortwave radiation	+0.39 (0.02)	+0.24 (0.16)	+0.16 (0.53)	+0.14 (0.59)
Net longwave radiation	−0.73 (0.00)	−0.65 (0.00)	−0.68 (0.00)	−0.67 (0.00)
Downwelling longwave Radiation	−0.34 (0.04)	−0.22 (0.21)	−0.10 (0.69)	−0.09 (0.72)
Upwelling longwave radiation	−0.50 (0.00)	−0.37 (0.02)	−0.47 (0.06)	−0.39 (0.12)
	+0.45 (0.01)	+0.42 (0.01)	+0.65 (0.00)	+0.55 (0.02)

^aWhen applicable, correlations are calculated using two atmospheric reanalyses and time periods. Bold values are significant at $p < 0.05$ (p values are in parentheses and assume independent observations). Radiation fluxes are defined as positive downward.

with net and downwelling shortwave radiation are no longer significant, nor are those with the net and downwelling longwave radiation. By contrast, while based on only a short record, there is an impressively strong correlation (−0.80) between the retreat date and the Bering Strait heat inflow averaged over the months April through June (at which time the heat flux is in the rising phase of its seasonal cycle).

As already introduced, the Bering Strait heat inflow has long been implicated in the seasonal melt back of ice, at least in a qualitative sense [Fedorova and Yankina, 1963; Paquette and Bourke, 1974; Ahlnas and Garrison, 1985; Spall, 2007; Woodgate *et al.*, 2010, 2012]. The average annual heat inflow over the 1998–2013 period from the A3 mooring data of 4.1×10^{20} J (with the stratification and ACC correction) represents the energy equivalent of melting 2.6 m of ice averaged over the Chukchi Sea shelf region (511,250 km²) and excursions of 1×10^{20} J, equating to about 0.6 m of ice, appear to be common in the observed record (Figure 8). Calculations presented by Woodgate *et al.* [2010] using the methodology of Perovich *et al.* [2007] suggest that the oceanic heat flux is comparable to the magnitude of the incoming shortwave radiation to the Chukchi Sea. The observed trend in the heat inflow of 5.5×10^{18} J per year (about 1% per year compared to the mean), if completely applied to the bottom of the ice in the Chukchi Sea study region, corresponds to about 0.034 m of ice melt per year.

These comparisons indicate the quantity of heat involved, but they do not show all this heat is used to melt ice in the Chukchi Sea. As discussed by Woodgate *et al.* [2010], likely only a fraction of this heat goes to melt ice in the Chukchi Sea. The rest may be lost to the atmosphere in the Chukchi Sea or transported to the Arctic, where it either melts ice, warms the atmosphere, or is sequestered in the Pacific Summer Water Layer in the Arctic [see Timmermans *et al.*, 2014]. (As discussed in Woodgate *et al.* [2012], only a small fraction, rough estimates suggest likely less than 1/4, is sequestered in the Pacific Summer Water in the western Arctic.) However, it is clear that all this heat must be lost somewhere, either through melting or escaping to the atmosphere, because by the time that the Pacific waters leave the Arctic Ocean they are known to be at the freezing point [Steele *et al.*, 2004].

The relationship between the complex pattern of the ice edge retreat and the known flow patterns of the waters in the Chukchi noted in section 3.1 provides observational evidence for a role of the oceanic heat flux (see Figure 2). Spall [2007], from studies with a regional ice-ocean model, concluded that “The ice melt pattern and timing is strongly influenced by advection through Bering Strait.” Woodgate *et al.* [2010] argue that, along with acting as a trigger for the onset of the seasonal melt back in the Chukchi Sea, by providing a subsurface heat reservoir for much of the Western Arctic, the Bering Strait heat inflow may also influence ice extent/thickness over a large area. Their study discussed the relationship between the large annual inflow recorded for 2007 ($\sim 5.3 \times 10^{20}$ J including an adjustment for stratification and the ACC) and the (then) record low September ice extent for the Arctic as a whole.

4.3. Correlations With Advance Day

Table 2 presents correlations between the physical variables and the date of sea ice advance. While the positive correlations between sea ice advance and both 2 m temperature and downwelling longwave radiation for July through September are logically explained in that the advance should be delayed when the system is warmer, the relationship is two-way because the presence of open water will also foster warmer and

Table 2. Pearson Correlations Between Detrended Time Series of Advance Day and Retreat Day, As Well Seasonal Oceanic, Surface Radiation, and Atmospheric Variables Averaged for July Through September^a

Variable	Full Record (1979–2014)		1991–1992, 1998–2013	
Retreat day		−0.58 (0.000)		−0.31 (0.208)
Bering Strait heat inflow		N/A		+0.67 (0.002)
	MERRA	ERA-Interim	MERRA	ERA-Interim
10 m meridional wind	+0.15 (0.37)	+0.15 (0.37)	+0.27 (0.27)	+0.32 (0.20)
2 m Temperature	+0.72 (0.00)	+0.69 (0.00)	+0.65 (0.00)	+0.57 (0.01)
Net allwave radiation	+0.52 (0.00)	+0.56 (0.00)	+0.51 (0.03)	+0.70 (0.00)
Net shortwave radiation	+0.41 (0.01)	+0.53 (0.00)	+0.37 (0.13)	+0.59 (0.01)
Downwelling shortwave radiation	−0.10 (0.55)	+0.04 (0.82)	+0.09 (0.71)	+0.61 (0.01)
Upwelling shortwave radiation	+0.67 (0.00)	+0.66 (0.00)	+0.47 (0.05)	+0.13 (0.62)
Net longwave radiation	−0.17 (0.31)	−0.15 (0.39)	−0.01 (0.98)	+0.09 (0.74)
Downwelling longwave radiation	+0.37 (0.02)	+0.50 (0.00)	+0.46 (0.05)	+0.52 (0.03)
Upwelling longwave radiation	−0.74 (0.00)	−0.70 (0.00)	−0.68 (0.00)	−0.50 (0.04)

^aWhen applicable, correlations are calculated using two atmospheric reanalyses and time periods. Bold values are significant at $p < 0.05$ (p -values are in parentheses and assume independent observations). Radiation fluxes are defined as positive downward.

moister air near the surface (surface warmth is manifested in the strong correlation with the upwelling longwave radiation). The positive correlation with upwelling shortwave simply suggests that when sea ice advances later, the surface albedo is lower and less shortwave radiation is reflected. Apart for the 17 year period from ERA-Interim, the correlation between the advance date and downwelling shortwave radiation is weak. This may represent the effects of the averaging period, which combines the middle of summer (July), when the cloud radiative effect tends to be negative (clouds cool the surface), with later in the season, when the cloud radiative effects tend back toward positive [Curry and Ebert, 1992].

From the 17 year record, note also the strong correlation (~ 0.67) between ice advance and the July through September Bering Strait inflow. As introduced in section 2.5, this correlation is complicated by the presence of seasonal autocorrelation in the inflow time series, viz, there is a correlation of 0.77 between the April through June inflow and the July through September inflow. Since the April through June inflow also influences the timing of sea ice retreat, this means that the retreat date and the July through September Bering Strait heat inflow cannot be viewed as independent predictors of sea ice advance. Interestingly, and reflecting the autocorrelation (persistence) in the inflow time series, the retreat date and the July through September inflow are significantly correlated at -0.56 .

There is also a fairly high correlation of -0.58 between the detrended time series of retreat and advance. We interpret this correlation as manifesting influences of albedo feedback and ocean heat uptake in spring and summer [Perovich *et al.*, 2007; Steele *et al.*, 2008; Stammerjohn *et al.*, 2012; Stroeve *et al.*, 2014] as well as the effects of variability in the northward heat flux through the Bering Strait. Regarding the ocean heat uptake and albedo feedback, as solar radiation increases and air temperatures rise in spring, surface melt lowers the surface albedo, accelerating ice melt. Eventually, dark open waters are exposed, becoming more extensive as the melt season progresses. These dark open water areas readily absorb solar radiation, increasing internal energy storage in the ocean mixed layer (about the top 20 m of the ocean). Before sea ice can form again in autumn, this mixed-layer heat must be lost to the atmosphere and to space via turbulent heat fluxes and radiation. Even in the absence of any trends, if the retreat date in a given year is earlier than average (e.g., via a stronger Bering Strait heat inflow or a random atmospheric forcing), the seasonal ocean heat uptake increases. This is because (a) earlier surface melt leads to an earlier drop in the ice albedo, meaning earlier and longer exposure of open water in areas that normally open later in the year, and (b) open water is exposed in areas that in a typical year would stay ice covered. As the spring-summer energy uptake increases, so will the delay in autumn ice growth because it takes longer for the ocean to lose the absorbed heat. An unusually late retreat will have the opposite effect.

The same argument logically holds regarding the response to external forcing. As part of an interhemispheric study of regions of rapid sea ice change, Stammerjohn *et al.* [2012] examined the correlation between detrended time series of retreat and advance for a combined eastern Siberian, Chukchi, and western Beaufort Sea sector for the period 1979–2011. The day of retreat and advance was determined for each 25 km grid cell in the passive microwave record. The stronger correlation they obtained of -0.81 may relate to the use of a broader spatial area for analysis than the Chukchi Sea region analyzed

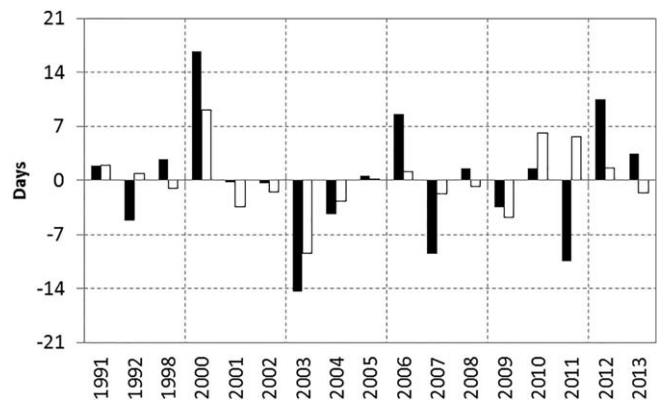


Figure 9. Detrended anomalies of retreat day (black, positive means a late retreat and negative means an early retreat) and model residuals (white).

optimal predictive capability for ice retreat day (RD) while maintaining physical and statistical integrity of the proposed model. The model with the greatest explanatory power turns out to only include the detrended April through June Bering Strait heat inflow (BHI):

$$RD = \alpha + \beta(BHI). \quad (1)$$

This model has a total explained variance of $R^2 = 0.68$ with 15° of freedom, meaning that it accounts for about two thirds of the variance in retreat day not described by the trend. The coefficient, beta, for Bering Strait heat inflow is -3.42 ± 1.17 days/TW (95% confidence interval; $p = 0.000$). The performance of this model compared to the trend line for each year is shown in Figure 9 by plotting the detrended time series of retreat day (black) along with the model residuals (white). Six of 17 detrended values are a week or more away from the actual retreat day, but only two of the model residuals exceed 7 days (2000 and 2003). Over half of all model estimates are within 2 days of the actual retreat day. Additionally, the 4 years with the earliest detrended retreat day (1992, 2003, 2007, and 2011) match the 4 years with the largest positive anomalies in the detrended Bering Strait heat inflow. The 4 years with the latest detrended retreat day (2000, 2006, 2012, and 2013) had the largest negative anomalies in detrended Bering Strait heat inflow. No other potential predictor from Table 1 matches so consistently.

Years for which the Bering Strait heat inflow alone cannot predict the timing of sea ice retreat to within a week likely reflect atmospheric influences. For example, the second lowest downwelling longwave radiation over these 17 years based on the reanalysis data was in 2000, when sea ice retreated later than predicted by Bering Strait heat inflow. The downwelling longwave flux was especially high in 2003, when sea ice retreated earlier than predicted by Bering Strait heat inflow. Interestingly, the model with the lowest BIC value (see section 2.5) included both downwelling longwave radiation and the meridional wind as predictors in addition to the Bering Strait heat inflow. However, while having the lowest BIC, this model was biased by several outliers and produced heteroskedastic residuals. Atmospheric influences on sea ice retreat are examined more closely in case studies for 2000 and 2003 in section 6.

5.2. Linear Model for Advance Day

The best overall model for explaining variance in the detrended advance day (AD) is

$$AD = \alpha + \beta_1(BHla) + \beta_2(RD), \quad (2)$$

where BHla is the detrended July through September Bering Strait heat inflow calculated after first subtracting the autocorrelation with the April through June inflow (see section 4.3), and RD is the detrended retreat day. Using ERA-Interim data, a more complicated model was preferred, but this two-variable model had a lower average BIC (and higher average R^2) between the two reanalyses.

Overall, this model has a total explained variance of $R^2 = 0.67$ with 14° of freedom, meaning that it accounts for about two-thirds of the variance in advance day not described by the long-term trend. Details presented in Table 3 show that again the dominant predictor is the Bering Strait heat inflow. This is shown by its higher partial r^2 value of 0.57, meaning that the explained variance would drop to 0.10 without Bering Strait

here. It may also reflect methodological differences. They performed a retreat and advance analysis grid cell by grid cell and then averaged the results, whereas we average the concentration for the entire Chukchi Sea shelf region, and then perform a retreat and advance analysis based on a concentration threshold of 30%.

5. Linear Statistical Models

5.1. Linear Model for Retreat Day

We apply the rigorous model selection process outlined in section 2.5 to identify parameters that provide the

Table 3. Coefficients (With 95% Confidence Interval), p Values, and Partial r^2 Values for Models Describing Detrended Advance Day Using Equation (2)^a

Variable	Coefficient	p value	Partial r^2
Intercept (days)	$+0.07 \pm 4.39$	0.98	N/A
Retreat day	-0.67 ± 0.59	0.04	0.12
Bering Strait heat inflow (TW)	$+3.79 \pm 1.49$	0.00	0.57

^aAll variables are detrended. Bering Strait heat inflow is a seasonal average for July through September with seasonal autocorrelation removed. Observations are from the 17 years for which all data are available (1991–1992, 1998, 2000–2013). Significant coefficients ($p < 0.05$) are bold.

1991) is only 15 days. Of the 4 years with the earliest advance compared to the trend line (the detrended value for advance is +31 days, while the model residual is only +1 day), pairing the strongest detrended Bering Strait heat inflow on record with the earliest detrended retreat day for the same period. Also interesting is that the summer atmospheric circulation, featuring positive SLP anomalies over the northern Beaufort Sea and negative SLP anomalies over northeastern Eurasia, led to persistent warm northward winds in the Chukchi Sea. While this wind pattern was key in forcing that summer's Arctic sea ice loss [e.g., Stroeve *et al.*, 2012], it may well have also favored a strong Bering Strait inflow, although in the annual mean, the 2007 winds in the strait were comparable to 2006. The year for which sea ice advanced especially late (1991) sees less improvement (+22 to +15 days) and is examined as a case study.

Regarding 2007, recall that *Woodgate et al.* [2010] discussed a link between the (then) record low September sea ice extent for the Arctic as a whole and the large Bering Strait heat inflow for this year. This year represents the most dramatic improvement from the trend line (the detrended value for advance is +31 days, while the model residual is only +1 day), pairing the strongest detrended Bering Strait heat inflow on record with the earliest detrended retreat day for the same period. Also interesting is that the summer atmospheric circulation, featuring positive SLP anomalies over the northern Beaufort Sea and negative SLP anomalies over northeastern Eurasia, led to persistent warm northward winds in the Chukchi Sea. While this wind pattern was key in forcing that summer's Arctic sea ice loss [e.g., Stroeve *et al.*, 2012], it may well have also favored a strong Bering Strait inflow, although in the annual mean, the 2007 winds in the strait were comparable to 2006. The year for which sea ice advanced especially late (1991) sees less improvement (+22 to +15 days) and is examined as a case study.

To summarize, based on a 17 year record and viewed with the other caveats discussed above, as with retreat, variability in the Bering Strait heat inflow appears to be key in predicting the date of ice advance. The remaining unexplained variance could be due to a number of factors. Although neither air temperature nor meridional wind velocity are used as predictors in the final retreat and advance models, it is well known that the September Arctic ice extent, on both a regional basis or for the Arctic as a whole, is strongly shaped by patterns of summer atmospheric circulation [e.g., Rogers *et al.*, 1978; Serreze *et al.*, 1989; Serreze *et al.*, 1995; Wang *et al.*, 2009; Zhang *et al.*, 2013; Serreze *et al.*, 2016]. With respect to the Chukchi Sea, the atmospheric link is also complicated in that the wind pattern can influence the Bering Strait inflow [*Woodgate et al.*, 2015]. Atmospheric influences are examined below in four case studies. First is 2000, which had the strongest positive residual from the retreat model (+9 days). Second is 2003, which had the strongest negative residual from the retreat model (−9 days). Third is 1991, which had the largest positive advance date residual (+15 days). Last is for 1992, which was tied with 2004 for the largest negative advance date residual (−13 days).

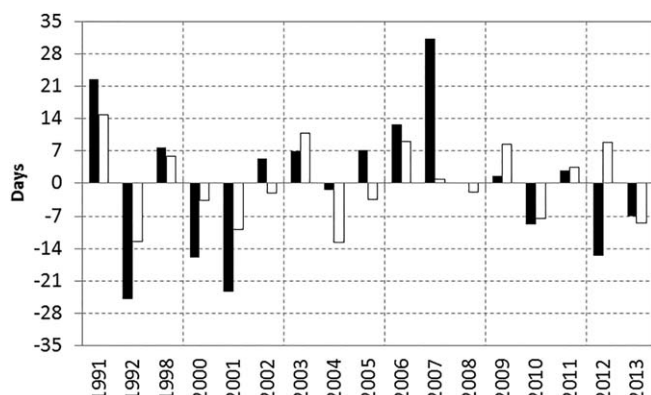


Figure 10. Detrended anomalies of advance day (black, positive means a late advance and negative means an early advance) and model residuals (white).

heat inflow. By contrast, excluding retreat day (partial $r^2 = 0.12$) would only reduce the explained variance to 0.55.

The graph of detrended values of advance day (black) compared to the model residuals (white) follows in Figure 10. In particular, note how although 4 years show the advance day lying more than 3 weeks away from the trend line, the largest residual from the model (in

1991) is only 15 days.

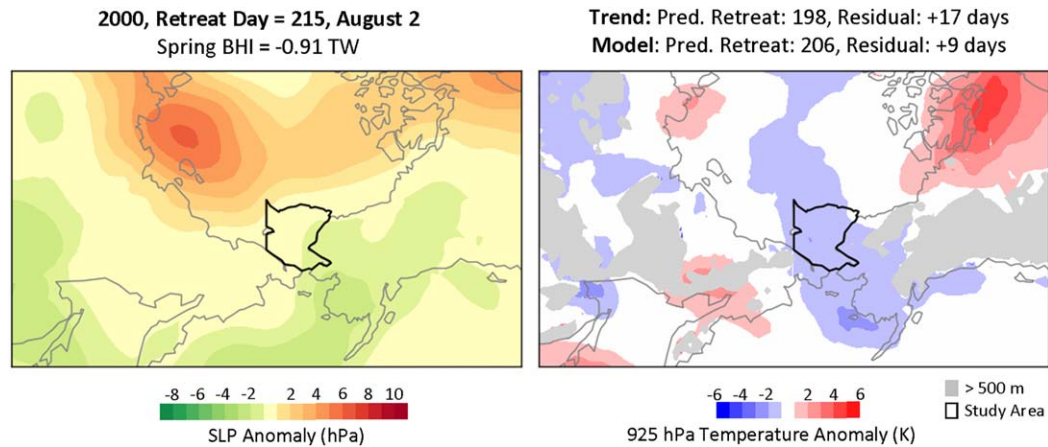


Figure 11. Sea level pressure and 925 hPa anomaly fields for 4 July through 2 August 2000, corresponding to the 30 day period prior to sea ice retreat. In the temperature plot, areas where the 925 hPa level intersects the local surface are shown in gray. Also indicated is the sea ice retreat date, the detrended Bering Strait heat inflow (BHI) for April through June and (above the right-hand figure) the predicted retreat day and its residual based in the linear trend and from the linear model.

Strait heat inflow of -0.91 TW. Fields of anomalies in SLP and 925 hPa temperature from MERRA averaged for the 30 day period prior to the observed retreat date (Figure 11) show a positive pressure anomaly centered over the Laptev Sea, partnered with a weak negative SLP anomaly in the north Pacific Ocean that together favored southward wind anomalies in the Chukchi Sea and air temperatures that were lower than average. These conditions may have delayed sea ice retreat both by fostering advection of ice into the Chukchi Sea from the Beaufort Sea and by limiting surface melt.

6.2. Case Study 2: 2003

In 2003, sea ice retreated 9 days earlier than predicted by the Bering Strait heat inflow. As in the previous case study for the year 2000, SLP anomalies during the 30 days before retreat were positive over the Arctic Ocean and negative over the north Pacific Ocean; however, longitudinal differences in these pressure anomaly features led to a very different result in the Chukchi Sea (Figure 12). Instead of sitting over the Laptev Sea as in 2000, the positive anomaly on 2003 was focused over the central Arctic Ocean. Instead of extending from the North Pacific over Alaska, the negative SLP anomaly was shifted toward Russia. This promoted wind anomalies from the south and corresponding warm conditions in the Chukchi Sea. Winds from the south will also tend to transport water vapor into the regions, increasing the downwelling longwave radiation flux [Mortin *et al.*, 2016].

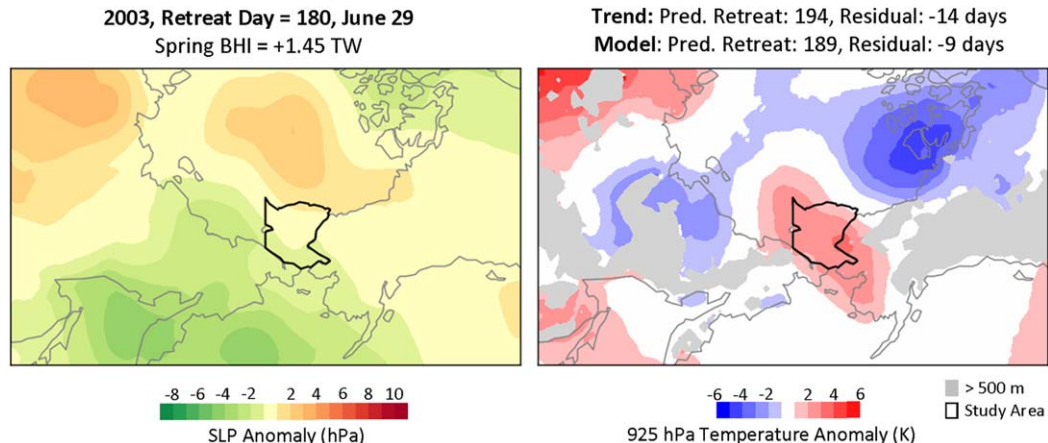


Figure 12. Sea level pressure and 925 hPa anomaly fields for 31 May through 29 June 2003, corresponding to the 30 day period prior to sea ice retreat. In the temperature plot, areas where the 925 hPa level intersects the local surface are shown in gray. Also indicated is the sea ice retreat date, the detrended Bering Strait heat inflow (BHI) for April through June and (above the right-hand figure) the predicted retreat day and its residual based in the linear trend and from the linear model.

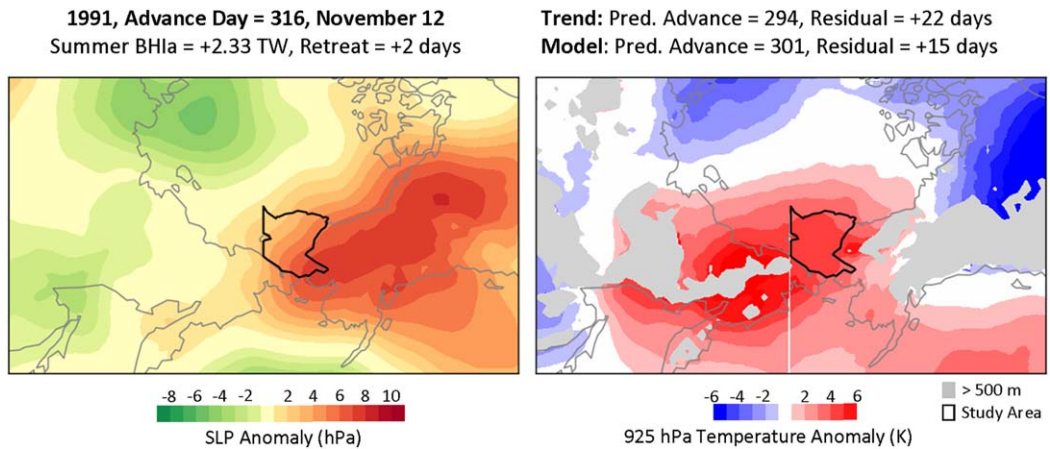


Figure 13. Sea level pressure and 925 hPa anomaly fields for 14 October through 12 November 1991, corresponding to the 30 day period prior to sea ice retreat. In the temperature plot, areas where the 925 hPa level intersects the local surface are shown in gray. Also indicated is the sea ice retreat date, the detrended Bering Strait heat inflow (BH_{1a}) for April through June and (above the right-hand figure) the predicted retreat day and its residual based in the linear trend and from the linear model.

6.3. Case Study 3: 1991

Similar arguments can be made for the years showing the largest model residuals for sea ice advance, such as 1991 (Figure 13). Recall that for this year, the predicted advance date was +19 days, that is, the advance was much later than predicted. This is likely related to the very warm conditions over the 30 days prior to advance. Note the strong positive temperature anomalies covering a broad area extending from eastern Eurasia eastward into the Beaufort Sea, associated with a strong positive anomaly in SLP centered over Alaska and the Yukon. While the positive temperature anomalies over the Chukchi Sea would have helped to delay autumn freezeup, they are also likely in part driven by the open water itself as the ocean loses the energy that it gained in summer back to the atmosphere (and is then radiated to space). The summer Bering Strait heat inflow was below average in the summer of 1991.

6.4. Case Study 4: 1992

The year 1992 (Figure 14) stands in sharp contrast. The open water period was only 70 days. This was almost entirely the result of an early advance day of 27 September, which was 24 days early with respect to the trend line still 13 days earlier than predicted by the linear model. At least qualitatively, conditions averaged for the 30 day period prior to advance offer a clue. The SLP field for this period features strong positive

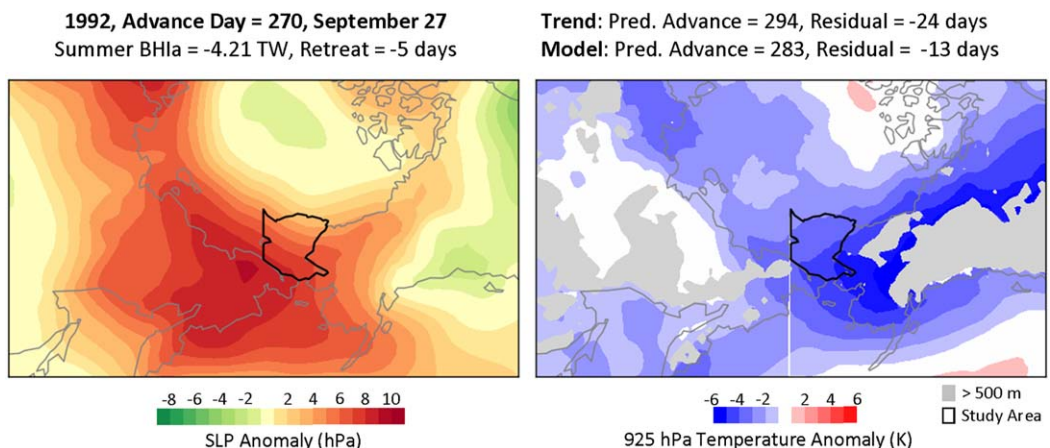


Figure 14. Sea level pressure and 925 hPa anomaly fields for 29 August through 27 September 1992, corresponding to the 30 day period prior to sea ice retreat. In the temperature plot, areas where the 925 hPa level intersects the local surface are shown in gray. Also indicated is the sea ice retreat date, the detrended Bering Strait heat inflow (BH_{1a}) for April through June and (above the right-hand figure) the predicted retreat day and its residual based in the linear trend and from the linear model.

anomalies aligned along the coast of northern Eurasia. The anomalous pressure gradient favored a more southward transport of ice into the Chukchi Sea. The anomalous surface wind component blowing from the Eurasian coastal seas (as opposed to from the warm land) is also consistent with the negative temperature anomalies inhibiting melt.

7. Conclusions

The observed links between (a) seasonal ice retreat and the April through June Bering Strait heat inflow, (b) ice retreat and advance, and (c) seasonal ice advance and the summer Bering Strait heat inflow, are all relevant in developing an operational predictive model of the open water period in the Chukchi Sea. Spring temperatures, the downwelling longwave radiation, and atmospheric circulation patterns may also influence the retreat date, but for both sea ice retreat and advance, the Bering Strait heat inflow is the single most important predictor. However, developing a practical operational model presents many challenges. The Bering Strait heat inflow time series is only 17 years long. Additionally, for predicting the advance date using the combination of the retreat date and the summer (July through September) Bering Strait heat inflow, a problem arises in that the retreat date is related to the spring Bering Strait heat inflow, which is in turn correlated with the summer inflow. Although removing the autocorrelation between the spring and summer inflow largely addresses this issue, more sophisticated methods applied to a longer time series may offer some improvement. To provide a sufficient lead time to supporting shipping activity in the area, it would also be necessary to use data from earlier in the year, for example, using the March through May heat inflow as a predictor of the retreat date as opposed to April through June; this can be addressed in a follow-on study.

Along these lines, a very practical need is much more timely acquisition of Bering Strait inflow data (e.g., at a 1 month time lag or less) than is presently the case. Environmental conditions (especially biofouling), dictate that one must periodically retrieve the moorings (typically in summer) to get the data. The use of surface floats on the moorings (from which data could be transmitted) is impractical as they would be destroyed by the sea ice in winter. Autonomous floats are also unsuited for the task as they would be rapidly carried away from the strait by the strong currents, and similarly, undersea gliders currently have insufficient station keeping in such strong currents in shallow water, and would also need to find ice-free zones for communications. Instead, other satellite proxies are being investigated, but so far with limited success. *Woodgate et al. [2012]* conclude that interannual change in Bering Strait fluxes can still only be adequately assessed with in situ measurements.

Also, while the observed trends in ice retreat, advance, and the open water period in the Chukchi Sea are consistent with external forcing (i.e., global warming) and are likely to continue, a link between external forcing and the trend in the Bering Strait heat inflow is by no means clear. A continued rise in ocean temperature, by itself, should translate into a rise in the Bering Strait heat inflow, but one must also consider potential changes in the volume flow linked to the Pacific-Atlantic pressure head and local winds. Finally, predictability of the advance date in particular will likely always be limited by the largely unpredictable nature of summer atmospheric circulation patterns over the Arctic Ocean beyond the 7–10 day time scale. The present study nevertheless lays a potential path forward to predict ice conditions in this increasingly critical region.

Acknowledgments

This study was supported by NSF grant PLR 1417016, PLR 130424, PLR 1304052, the NSF Graduate Research Fellowship Program grant DGE 1144053, and the Earth Science Interdisciplinary Center (ESSIC) Task 683. Data from the Bering Strait moorings (currently funded by NSF-AON, with prior support from NFS, ONR, NOAA-RUSALCA, and MMS), are available via the Bering Strait project website <http://psc.apl.washington.edu/BeringStrait.html> and the National Centers for Environmental Information <https://www.ndc.noaa.gov>, formerly the National Oceanographic Data Center. MERRA data are available at <http://disc.sci.gsfc.nasa.gov/mdi/> while ERA-Interim data are available at <http://www.ecmwf.int/en/research/climate-reanalysis/era-interim>. The passive microwave sea ice concentration fields, as well as fields of sea ice motion and age are available through the National Snow and Ice Data Center at <http://nsidc.org/>.

References

- Aagaard, K., T. J. Weingarter, S. Danielson, R. A. Woodgate, G. C. Johnson, and T. Whitledge (2006), Some controls on flow and salinity in Bering Strait, *Geophys. Res. Lett.*, 33, L19602, doi:10.1029/2006GL026612.
- Ahlnas, K., and G. R. Garrison (1985), Satellite and oceanographic observations of the warm coastal current in the Chukchi Sea, *Arctic*, 37, 244–254.
- Babb, D. G., R. J. Galley, M. G. Asplin, J. V. Lukovich, and D. G. Barber (2013), Multiyear sea ice export through the Bering Strait during winter 2011–2012, *J. Geophys. Res. Oceans*, 118, 5489–5503, doi:10.1002/jgrc.20383.
- Comiso, J. C. (2012), Large decadal decline of the Arctic multi-year ice cover, *J. Clim.*, 25, 1176–1193, doi:10.1175/JCLI-D-11-00113.1.
- Curry, J. A., and E. E. Ebert (1992), Annual cycle of radiation fluxes over the Arctic Ocean: Sensitivity to cloud optical properties, *J. Clim.*, 5, 1267–1280.
- Dee, D. P., et al. (2011), The ERA-Interim reanalysis: Configuration and performance of the data assimilation system, *Q. J. R. Meteorol. Soc.*, 137, 553–597, doi:10.1002/qj.828.
- Fedorova, A. P., and A. S. Yankina (1963), The passage of Pacific Ocean water through the Bering Strait into the Chukchi Sea, *Deep Sea Res. Oceanogr. Abstr.*, 20, 217–224.
- Fetterer, F., K. Knowles, W. Meier, and M. Savoie (2002), *Sea Ice Index*, Natl. Snow and Ice Data Cent., Boulder, Colo. [Available at <http://nsidc.org/data/G02135>.]
- Fowler, C., W. J. Emery, and J. Maslanik (2004), Satellite-derived evolution of Arctic sea ice age: October 1978 to March 2003, *IEEE Geosci. Remote Sens. Lett.*, 1, 71–74, doi:10.1109/LGRS.2004.824741.

Francis, J. A., and S. J. Vavrus (2012), Evidence linking Arctic amplification to extreme weather in middle latitudes, *Geophys. Res. Lett.*, **39**, L06801, doi:10.1029/2012GL051000.

Kapsch, M.-L., R. G. Graversen, M. Tjernström, and R. Bintanja (2016), The effect of downwelling longwave and shortwave radiation on Arctic summer sea ice, *J. Clim.*, **29**, 1143–1159, doi:10.1175/JCLI-D-15-0238.1.

Lindsay, R., M. Wenshahan, A. Schweiger, and J. Zhang (2014), Evaluation of seven different atmospheric reanalysis products in the Arctic, *J. Clim.*, **27**, 2588–2606, doi:10.1175/JCLI-D-13-00014.1.

Maslanik, J. A., C. Fowler, J. Stroeve, S. Drobot, J. Zwally, D. Yi, and W. Emery (2007), A younger, thinner Arctic ice cover: Increased potential for rapid extensive sea ice loss, *Geophys. Res. Lett.*, **34**, L24501, doi:10.1029/2007GL032043.

Maslanik, J., J. Stroeve, C. Fowler, and W. Emery (2011), Distribution and trends in Arctic sea ice age through spring 2011, *Geophys. Res. Lett.*, **38**, L13502, doi:10.1029/2011GL047735.

Moore, G. W. K. (2012), Decadal variability and recent amplification of the summer Beaufort Sea High, *Geophys. Res. Lett.*, **39**, L10807, doi:10.1029/2012GL051570.

Moore, S. E., and K. E. Laird (2006), Trends in sea ice cover within habitats used by bowhead whales in the western Arctic, *Ecol. Appl.*, **16**, 932–944, doi:10.1890/1051-0761(2006)016[0932:TISICW]2.0.CO;2.

Martin, J., G. Svensson, and R. G. Graversen (2016), Melt onset over Arctic sea ice controlled by atmospheric moisture transport, *Geophys. Res. Lett.*, **43**, 6636–6642, doi:10.1002/(ISSN)1944-8007.

Oceana and Kawerak (2014), Bering Strait marine life and subsistence use data synthesis, 499 pp., Juneau, Alaska. [Available at <http://oceana.org/news-media/publications/reports/the-bering-strait-marine-life-and-subsistence-data-synthesis>.]

Overland, J. (2009), Meteorology of the Beaufort Sea, *J. Geophys. Res.*, **114**, C00A07, doi:10.1029/2008JC004861.

Overland, J. E., J. A. Francis, E. Hanna, and M. Wang (2012), The recent shift in early summer atmospheric circulation, *Geophys. Res. Lett.*, **39**, L19804, doi:10.1029/2012GL053268.

Paquette, R. G., and R. H. Bourke (1974), Observations on the coastal current of arctic Alaska, *J. Mar. Res.*, **32**, 195–207.

Perlitz, J., M. Hoerling, and R. Dole (2015), Arctic tropospheric warming: Causes and linkages to lower latitudes, *J. Clim.*, **28**, 2154–2167, doi:10.1175/JCLI-D-14-00095.1.

Perovich, D. K., B. Light, H. Eicken, K. F. Jones, K. Runciman, and S. V. Nghiem (2007), Increasing solar heating of the Arctic Ocean and adjacent seas, 1979–2005: Attribution and the role of ice-albedo feedback, *Geophys. Res. Lett.*, **34**, L19505, doi:10.1029/2007GL031480.

Post, E., U. S. Bhatt, C. M. Bitz, J. F. Brodie, T. L. Fulton, M. Hebblewhite, J. Kerby, S. L. Kutz, I. Stirling, and D. A. Walker (2013), Ecological consequences of sea ice decline, *Science*, **341**, 519–524, doi:10.1126/science.1235225.

Raymond-Yakoubian, J., Y. Khokhlov, and A. Yarzutkina (2014), Indigenous knowledge and use of Bering Strait region ocean currents, final report, p. 126, Kawerak, Inc., Nome, Alaska. [Available at <http://www.kawerak.org/forms/nr/OC%20report%20for%20web.pdf>.]

Rienecker, M. M., et al. (2011), MERRA—NASA's modern-era retrospective analysis for research and applications, *J. Clim.*, **24**, 3624–3648, doi:10.1175/JCLI-D-00015.1.

Rogers, J. C. (1978), Meteorological factors affecting interannual variability of summertime ice extent in the Beaufort Sea, *Mon. Weather Rev.*, **106**, 890–897.

Schwarz, G. (1978), Estimating the dimension of a model, *Ann. Stat.*, **6**, 461–464.

Screen, J. A., and I. Simmonds (2010), The central role of diminishing sea ice in recent Arctic temperature amplification, *Nature*, **464**, 1334–1337.

Serreze, M. C., and A. P. Barrett (2011), Characteristics of the Beaufort Sea high, *J. Clim.*, **24**, 159–182, doi:10.1175/2010JCL3636.1.

Serreze, M. C., R. G. Barry, and A. S. McLaren (1989), Seasonal variations in sea ice motion and effects on sea ice concentration in the Canada Basin, *J. Geophys. Res.*, **94**(C8), 10,955–10,970.

Serreze, M. C., J. A. Maslanik, J. R. Key, R. F. Kokaly, and D. A. Robinson (1995), Diagnosis of the record minimum in Arctic sea ice area during 1990 and associated snow cover extremes, *Geophys. Res. Lett.*, **22**, 2183–2186.

Serreze, M. C., A. P. Barrett, J. C. Stroeve, D. M. Kindig, and M. Holland (2009), The emergence of surface-based Arctic amplification, *Cryosphere*, **3**, 9–11.

Serreze, M. C., J. Stroeve, A. P. Barrett, and L. N. Boisvert (2016), Summer atmospheric circulation anomalies over the Arctic Ocean and their influences on September sea ice extent: A cautionary tale, *J. Geophys. Res. Atmos.*, doi:10.1002/2016JD025161, in press.

Spall, M. A. (2007), Circulation and water mass transformation in a model of the Chukchi Sea, *J. Geophys. Res.*, **112**, C05025, doi:10.1029/2005JC003364.

Stammerjohn, S., R. Massom, D. Rind, and D. Martinson (2012), Regions of rapid sea ice change: An inter-hemispheric seasonal comparison, *Geophys. Res. Lett.*, **39**, L06501, doi:10.1029/2012GL080874.

Steele, M., J. Morison, W. Ermold, I. Rigor, M. Ortmeyer, and K. Shimada (2004), Circulation of summer Pacific halocline water in the Arctic Ocean, *J. Geophys. Res.*, **109**, C02027, doi:10.1029/2003JC002009.

Steele, M., W. Ermold, and J. Zhang (2008), Arctic Ocean surface warming trends over the past 100 years, *Geophys. Res. Lett.*, **35**, L02614, doi:10.1029/2007GL031651.

Stroeve, J. C., M. C. Serreze, M. M. Holland, J. E. Kay, J. A. Maslanik, and A. P. Barrett (2012), The Arctic's rapidly shrinking sea ice cover: A research synthesis, *Clim. Change*, **110**, 1005–1027, doi:10.1007/s10584-011-0101-1.

Stroeve, J. C., T. Markus, L. Boisvert, J. Miller, and A. Barrett (2014), Changes in Arctic melt season and implications for sea ice loss, *Geophys. Res. Lett.*, **41**, 1216–1225, doi:10.1002/2013GL058951.

Tang, Q., X. Zhang, X. Yang, and J. A. Francis (2013), Cold winter extremes in northern continents linked to Arctic sea ice loss, *Environ. Res. Lett.*, **8**, 014036, doi:10.1088/1748-9326/8/8/014036.

Timmermans, M.-L., A. Proshutinsky, E. Golubeva, J. M. Jackson, R. Krishfield, M. McCall, G. Platov, J. Toole, W. Williams, T. Kikuchi, and S. Nishino (2014), Mechanisms of Pacific Summer Water variability in the Arctic's central Canada Basin, *J. Geophys. Res.*, **119**, 7523–7548, doi:10.1002/2014JC010273.

United States Navy (2014), *The United States Navy Arctic Roadmap for 2014 to 2030*, 38 pp., Department of the Navy, Washington, D. C. [Available at www.navy.mil/docs/USN_arctic_roadmap.pdf.]

Wang, J., J. Zhang, E. Watanabe, M. Ikeda, K. Mizobata, J. E. Walsh, X. Bai, and B. Wu (2009), Is the dipole anomaly a major driver to record lows in Arctic summer sea ice extent? *Geophys. Res. Lett.*, **36**, L05706, doi:10.1029/2008GL036706.

Weingartner, T., K. Aagaard, R. Woodgate, S. Danielson, Y. Sasaki, and D. Cavalieri (2005), Circulation on the north central Chukchi Sea shelf, *Deep Sea Res., Part II*, **52**(24–26), 3150–3174, doi:10.1016/j.dsrr.2005.10.01.

Woodgate, R. A., K. Aagaard, and T. J. Weingartner (2005a), A year in the physical oceanography of the Chukchi Sea: Moored measurements from autumn 1990–1991, *Deep Sea Res., Part II*, **52**(24–26), 3116–3149, doi:10.1016/j.dsrr.2005.10.016.

Woodgate, R. A., K. Aagaard, and T. J. Weingartner (2005b), Monthly temperature, salinity and transport variability of the Bering Strait throughflow, *Geophys. Res. Lett.*, **32**, L04601, doi:10.1029/2004GL021880.

Woodgate, R. A., T. Weingartner, and R. Lindsay (2010), The 2007 Bering Strait oceanic heat flux and anomalous Arctic sea-ice retreat, *Geophys. Res. Lett.*, 37, L01602, doi:10.1029/2009GL041621.

Woodgate, R. A., T. Weingartner, and R. Lindsay (2012), Observed increases in Bering Strait oceanic fluxes from the Pacific to the Atlantic from 2001 to 2010 and their impacts on the Arctic Ocean water column, *Geophys. Res. Lett.*, 39, L24603, doi:10.1029/2012GL054092.

Woodgate, R. A., K. M. Stafford, and F. G. Prahls (2015), A synthesis of year-round interdisciplinary mooring measurements in the Bering Strait (1990–2014) and the RUSALCA years (2004–2011), *Oceanography*, 28, 46–67, doi:10.5670/oceanog.2015.57.

Wu, Q., J. Zhang, X. Zhang, and W. Tao (2014), Interannual variability and long-term changes of atmospheric circulation over the Chukchi and Beaufort seas, *J. Clim.*, 27, 4871–4889, doi:10.1175/JCLI-D-13-00610.1.

Zhang, J., R. Lindsay, A. Schweiger, and M. Steele (2013), The impact of an intense summer cyclone on 2012 Arctic sea ice retreat, *Geophys. Res. Lett.*, 40, 720–726, doi:10.1002/grl.50190.